Two-Dimensional Halide Perovskites for Emerging New- Generation Photo

Tang, Yingying; Cao, Xianyi; Chi, Qijin

Published in:
Two-dimensional Materials for Photodetector

Link to article, DOI:
10.5772/intechopen.71032

Publication date:
2018

Document Version
Publisher's PDF, also known as Version of record

Chapter 4

Two-Dimensional Halide Perovskites for Emerging New-Generation Photodetectors

Yingying Tang, Xianyi Cao and Qijin Chi

Additional information is available at the end of the chapter

http://dx.doi.org/10.5772/intechopen.71032

Abstract

Compared to their conventional three-dimensional (3D) counterparts, two-dimensional (2D) halide perovskites have attracted more interests recently in a variety of areas related to optoelectronics because of their unique structural characteristics and enhanced performances. In general, there are two distinct types of 2D halide perovskites. One represents those perovskites with an intrinsic layered crystal structure (i.e. MX_6 layers, M = metal and X = Cl, Br, I), the other defines the perovskites with a 2D nanostructured morphology such as nanoplatelets and nanosheets. Recent studies have shown that 2D halide perovskites hold promising potential for the development of new-generation photodetectors, mainly arising from their highly efficient photoluminescence and absorbance, color tunability in the visible-light range and relatively high stability. In this chapter, we present the summary and highlights of latest researches on these two types of 2D halide perovskites for developing photodetectors, with an emphasis on synthesis methods, structural characterization, optoelectronic properties, and theoretical analysis and simulations. We also discuss the current challenging issues and future perspective. We hope this chapter would add new elements for understanding halide perovskite-based 2D materials and for developing their more efficient optoelectronic devices.

Keywords: photodetector, halide perovskite, two-dimensional layered structure, nanoplatelet, and optoelectronic device

1. Introduction to photodetectors and halide perovskites

Photodetection techniques have demonstrated many important applications in a variety of fields or occasions, including medical X-ray imaging, ubiquitous visible light cameras, near-infrared medical imaging and short-wave infrared surveillance and machine vision [1–5]. Current photodetection relies primarily on conventional semiconductor materials with an

appropriate bandgap, capable of transducing photons with different energies into electrical signals for subsequent processing, image reconstruction and storage. Historically, silicon and III–V semiconductors have been most commonly used as photodiodes and phototransistors (**Figure 1**) [6–8]. However, these conventional inorganic semiconductors are broadband absorbers. Thus, they produce a broad spectral photoresponse that could complicate the architecture and fabrication of devices and makes it difficult in pure color replication. Since the discovery of electrical conductivity in doped polypyrrole in the 1960s [9] and myriads of small-molecule and polymeric conductors and semiconductors during the 1970s and 1980s, organic semiconductors have shown promising applications in solar cells, field-effect transistors (FET) and photodetectors [10–12]. However, engineering organic semiconductors with an optical bandgap below 1 eV remains a challenge, as well as their carrier mobility is normally low. In addition, most organic planar photodetectors suffer from slow response time (≥10 ms), high operation voltage (≥10 V) and lack of stability to UV light (190–350 nm) [13]. This has driven the development of colloidal quantum dot (CQD)-based photodetectors, such as CdS, CdSe and PbS [14–16], as a possible option to expand the range of optical path difference (OPD). In most CQD-based photodetectors, however, a compromise between carrier extraction and absorption efficiency is required in order to reduce the electrical volume of the photoactive material but without sacrificing absorption. More recently, metal-halide perovskites have emerged as new candidate materials for optoelectronic devices (solar cells in particular) with the conversion efficiency reaching over 20% [17]. It is thus expected that using metal-halide perovskites as the key material component could construct new-generation photodetectors. In general, perovskites are optically tunable from 390 to 790 nm via halide-exchange or quantum confinement effect (**Figure 1**), so that they possess an appropriate bandgap exhibiting a steep absorption edge and demonstrate remarkable efficiency in photo-generated charge collection [18–22]. These unique optical properties make halide perovskites play key roles in the recent rapid development of solar cells, which has also spawned the exploration of diverse applications of halide perovskites across the domain of photodetectors. Metal halide perovskite-based photodetectors could

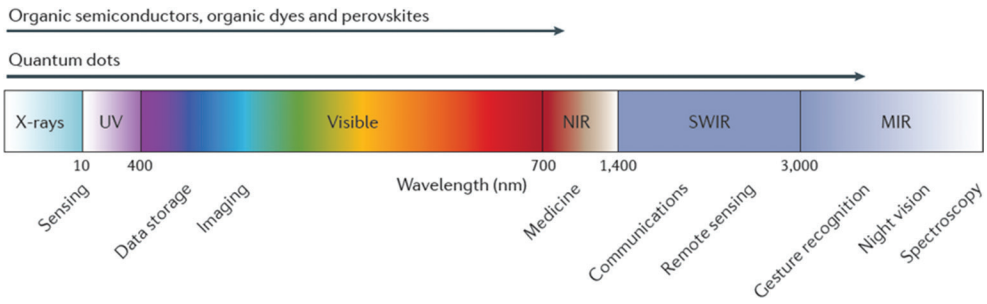

Figure 1. Schematic illustration of the wavelength region and potential application of semiconducting materials including organic semiconductors, organic dyes, halide perovskites and quantum dots. These semiconducting materials having the different applicable spectra region [8]. Abbreviation: UV, ultraviolet; NIR, near-infrared; MIR, mid-infrared; SWIR for short-wave infrared.

have the notable advantages such as ease of processing, tailorable optical property, good compatibility with flexible substrates and synergistic integration with complementary metal oxide semiconductors [23–26].

Compared to three-dimensional (3D) materials, two-dimensional (2D) materials, defined as crystals with very high aspect ratios and thicknesses corresponding to a few atomic layers, usually exhibit unique properties [27–30]. Graphene is the first example discovered with a true 2D atomic crystal, which is known by its high chemical stability [31] and large specific surface area [32]. In particular, graphene has a very high electronic conductivity [33] and absorbs the incoming radiation almost independent of wavelength [34], which can perform synergistic functionality in optoelectronic devices. Besides, other newly emerged 2D materials, such as hexagonal boron nitride (h-BN), [35] transition-metal dichalcogenides (TMDs) [36], layered metal oxides [37], and Venes (phosphorene and arsenene) [38, 39] have also attracted broad interests in various fields. Unlike above-mentioned 2D materials, however, 2D perovskites in the form of nanoplatelet (NPL) or nanosheet and layered-structure perovskites are ionic materials. This chemical bonding nature could endow them special properties distinguished from their 3D structures. For example, these 2D perovskites have an increased exciton binding energy, can reduce fluorescence decay time, and enhance absorption cross sections with respect to the bulk as well as having a notable optical nonlinearity [40–42]. Moreover, energy transfer in the stack of 2D perovskite sheets or platelets is significantly enhanced due to the large contact area between individual platelets. Note that the construction of 3D perovskites needs to match some critical parameters such as Goldschmidt's Tolerance Factor, ionic radii, charge balance and bonding/coordination preference, in order to produce stable structures. In 2D perovskites, in contrast, a remarkable structural tunability is feasible especially for the interlayer "A" cation length. This character provides a high flexibility for the design and synthesis of desirable 2D perovskite crystal structures with new physicochemical properties.

This chapter aims at summarizing recent advances and discussing current challenges and ongoing efforts in the development of 2D perovskite-based photodetectors. We *first* briefly overview recent research progress in 2D perovskites before focusing on the optoelectronic properties of 2D layered perovskite structures or perovskite nanoplatelets and nanosheets and photodetectors. We summarize a number of popular methods for the preparation of 2D perovskites, their structural characterizations and fabrication and tests of photodetectors. Also included is a brief discussion on theoretical simulations of electronic structures of halide perovskites for their perspective applications in future optoelectronic devices.

2. Design and preparation of 2D halide perovskites

To obtain desirable optical properties, the design and controlled synthesis of 2D metal-halide perovskites is a critical step. In this section, we focus on summarizing the recent progress in the synthesis of 2D halide perovskites.

2.1. Solution-processed methods

Some 2D halide perovskites can be prepared via solution-processed methods, which represent low-cost, flexible and efficient approach in many cases. For example, Sun et al. recently reported the synthesis of $CsPbBr_3$ nanostructures with different morphologies by adjusting different groups of acids and amines (**Figure 2a**) [43]. In the presence of hexanoic acid and octylamine, the nanocrystals can be tailored into spherical quantum dots. Nanocubes were generated under the coordination effects of oleic acid and dodecylamine, while nanoplatelets formed with the help of oleic acid and octylamine. The average size for these three types of nanostructures is 4.3, 9 and 100 nm, respectively. Their photoluminescence (PL) decay lifetime was determined to be in the range from several tens to hundreds of nanoseconds [43]. In another approach, Bekenstein et al. prepared colloidal nanoplatelets (NPLs) of $CsPbBr_3$ at

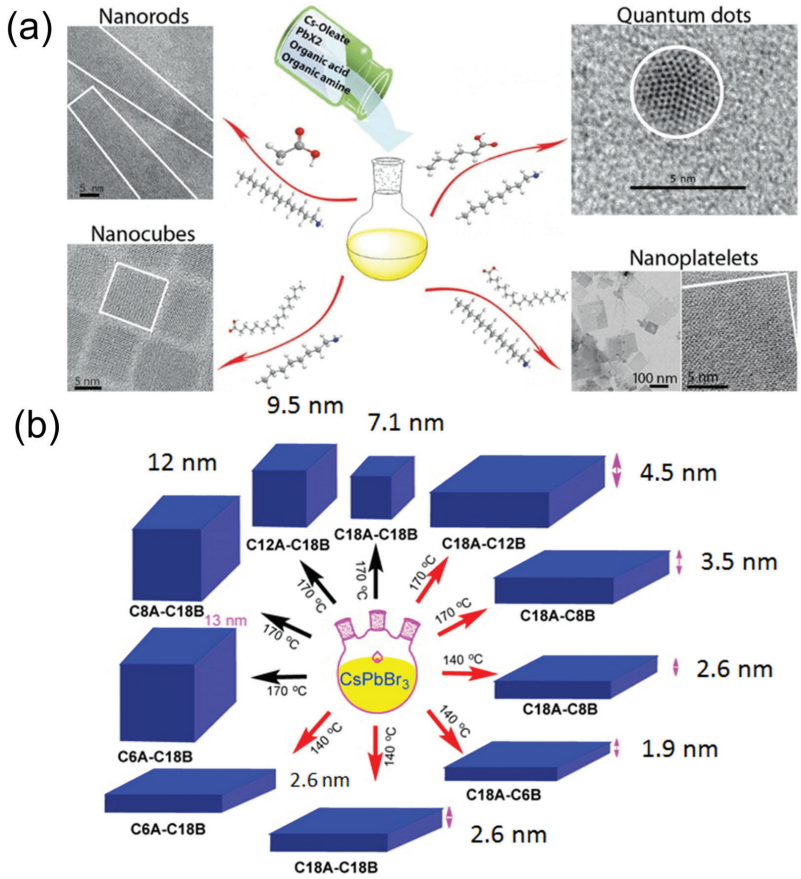

Figure 2. Summary of the synthesis methods for halide perovskite nanostructures. (a) Schematic view of the formation process of $CsPbX_3$ (X = Cl, Br, I) nanocrystals with different morphology [43]. (b) Morphology and size control of $CsPbBr_3$ nanocrystals through varying the temperature and surfactants [45].

elevated temperatures, in which hot Cs-oleate solution was quickly injected into the $PbBr_2$ solution containing octadecene, oleylamine and oleic acid [44]. The shape and thickness of $CsPbBr_3$ NPLs was roughly controllable by adjusting the injection temperature of Cs-oleate solution. Thin NPLs, thicker NPLs, nanocubes and large nanocubes together with nanowires were obtained under 90, 130, 150, 170–200°C, respectively. However, no nanocrystals are generated below 70°C. $CsPbBr_3$ NPLs obtained at 130°C have a lateral dimension of ~20 nm and a thickness of ~3 nm. PL spectra were tuned from 512 nm (5 unit cell thickness) to 405 nm (1 unit cell thickness). For those NPLs with 5, 4, and 3 unit cell thickness, the photoluminescence quantum yield (PLQY) is 84.4 ± 1.8, 44.7 ± 2.6 and 10 ± 0.5%, respectively. The perovskite NPLs can be further assembled into stacked columnar phases by concentrating NPLs solutions and large 2D sheets by diluting samples [44]. Pan et al. studied the effects of organic acid, base and cesium precursors on the morphology of $CsPbBr_3$ perovskite nanocrystals (**Figure 2b**) [45]. The use of shorter chain amines resulted in the formation of thin nanoplatelets, while using shorter chain carboxylic acids led to large-size nanocubes at high temperatures. Furthermore, using CsOAc as the Cs source can overcome the solubility problem that existed in Cs_2CO_3 precursor, showing superior performance, which allows the use of low boiling point reactants, such as acid or amine with chain length shorter than eight carbons. These findings have demonstrated the feasibility to tune the shape, size and optoelectronic properties of halide perovskites [45].

2.2. Vapor-phase methods

Vapor-deposition methods including chemical vapor deposition (CVD), van der Waals (VDW) epitaxy and other related methods are effective approaches to the preparation of high quality 2D nanocrystals especially for conventional semiconductors [46, 47]. These methods have now been attempted for the synthesis of 2D perovskites. Following is a brief summary with some representative examples illustrated.

Ha et al. first reported the preparation of $CH_3NH_3PbX_3$ nanoplatelets via a gas-solid heterophase reaction, [48] as illustrated in **Figure 3a**. By means of VDW epitaxy, lead halide nanoplatelets were initially grown on muscovite mica and then were converted into perovskites via gas-solid reaction with CH_3NH_3X. The resulting nanoplatelets had the lateral dimension in the range of 5–30 μm and the thickness from several atomic layers to several 100 nm. $CH_3NH_3PbI_3$ nanoplatelets exhibited a large diffusion length of ~200 nm (**Figure 3b**) [48]. Adding phenyl-C61-butyric acid methyl ester (PCBM) layer onto the $CH_3NH_3PbI_3$ platelets resulted in the reduction of PL lifetime from 6.8 ± 0.4 to 0.278 ± 0.004 ns. Besides, the electron-diffusion length was estimated to be 210 ± 50 nm, [49] which can be attributed to the high quality perovskites prepared from vapor-phase method. Wang et al. prepared crystalline 2D $MAPbCl_3$ perovskite thin platelets on muscovite mica using VDW epitaxy method, with the thickness of sub-10 nm and a few tens of micrometers in the lateral dimension (**Figure 3c**) [50]. Weak VDW interaction and delocalized bonding characters of ionic and metallic crystals play key roles in forming ultrathin and large-scale $MAPbCl_3$ platelets.

A single-step CVD approach was developed by Wang et al. to prepare all-inorganic halide perovskite, $CsPbX_3$ microplatelets [51]. The two types of precursor powders (PbX_2 and CsX)

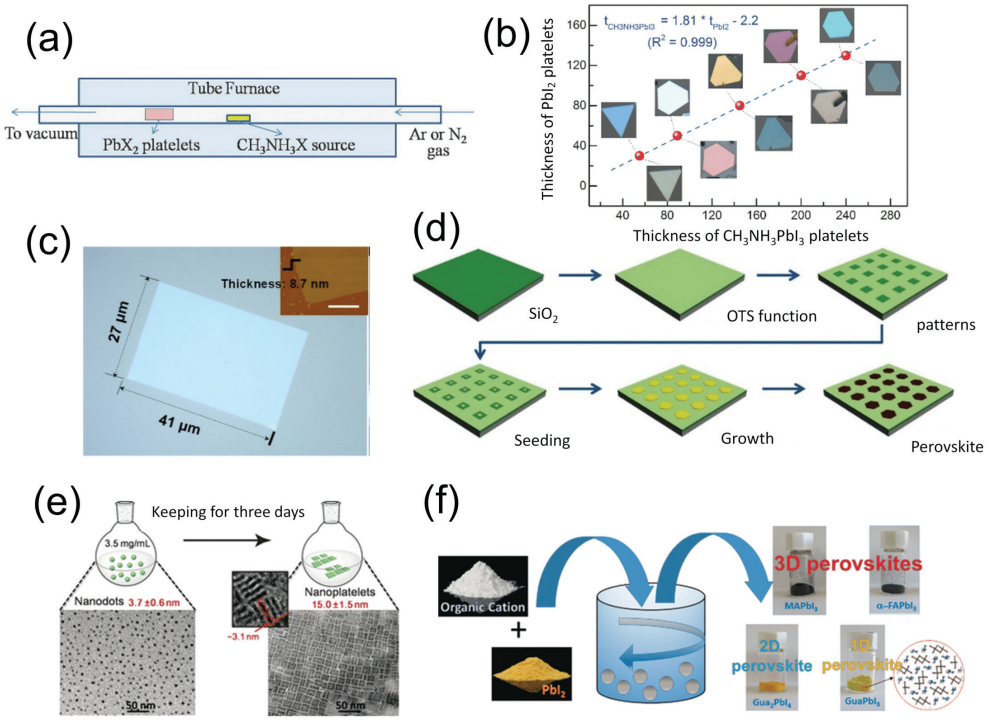

Figure 3. (a) Diagram of vapor-phase-transport system setup [48]. (b) Correlation of the thickness of PbI_2 and $CH_3NH_3PbI_3$ platelets [48]. The inset represents the optical image of $CH_3NH_3PbI_3$ platelets. (c) Optical image of an individual large-size ultrathin sheet [50]. The inset shows the thickness of the sheet by AFM measurement. (d) The procedure for preparing $CH_3NH_3PbI_3$ plates on a patterned substrate [52]. (e) Self-transformation of $CH_3NH_3PbBr_3$ nanodots to nanoplatelets [53]. The enlarged parts represent the corresponding TEM images of $CH_3NH_3PbBr_3$ nanocrystals. (f) Scheme of the mechanochemical synthesis for the 3D, 2D and 1D perovskites [54].

were mixed in a stoichiometric ratio and reacted in a home-built CVD system under controlled temperatures [51]. A quality factor up to 2863 was achieved in $CsPbX_3$ microplatelets-based gain medium and whispering gallery mode cavity, while the photodetector based on a sandwiched structure of graphene/CsPbX3 microplatelets/vertically stacked graphene displayed a high photoresponsivity $>10^5$ A/W. Similarly, Wang et al. demonstrated a two-step wafer-scale growth of large arrays of $CH_3NH_3PbI_3$ microplate crystals [52]. The SiO_2/Si substrate was functionalized by (octadecyl)trichlorosilane (OTS) forming a hydrophobic surface, followed by a selective growth of PbI_2 plates on the hydrophilic region generated by the oxygen-plasma treatment. Finally, perovskite platelets were obtained via immersing PbI_2 plates into CH_3NH_3I vapor (**Figure 3d**).

2.3. Other synthesis methods

Besides solution-processed and vapor-phase methods, other methods have also been attempted to prepare 2D metal halide perovskites such as self-organization synthesis and mechanochemical

approaches. Still, more alternative methods are in progress with the aim to control the morphology and thickness of 2D halide perovskites more effectively.

Liu et al. demonstrated the self-organization process for the transformation of $CH_3NH_3PbBr_3$ nanodots (NDs) to NPLs [53]. In detail, the $CH_3NH_3PbBr_3$ NDs were dissolved in a nonpolar solvent and aged in darkness (**Figure 3e**). The thickness of resulting $CH_3NH_3PbBr_3$ NPLs is similar to the size of original NDs, but the lateral dimension is about fourfold to the original NDs. Theoretical simulations show that the side-side orientation with the coordination between electrostatic and van der Waals interactions is favored during the self-organization process. The resulting NPLs loaded into a polymer matrix (4-methyl-1-pentene, TPX) displayed cos/sin intensity dependence on the polarizer angles for the PL emission. In addition, this method offers a new way for controlling the shape of perovskite-based nanomaterials with polarized emission [53]. Jodlowski et al. reported the preparation of a bi-dimensional (i.e. 2D) perovskite (Gua_2PbI_4) using a mechanochemical synthesis approach (**Figure 3f**) [54]. The precursors of PbI_2 and MAI were mixed in a 1:1 molar ratio inside a ball mill under ambient conditions to produce polycrystalline powders. This synthesis process featured solventless environment, swiftness, simplicity, reproducibility and promising potential for exploring the alternative design of various perovskite nanostructures [54].

3. Structural characteristics and analysis of 2D halide perovskites

3.1. General structural features

In general, there are two kinds of 2D metal halide perovskites. One is the intrinsically layered crystal structure, which are electronically "2D" due to the quantum confinement in the layers composed of MX_6 octahedra separated by organic cations. The other is those perovskites with 2D nanostructured morphology but intrinsically have 3D structures.

In the 2D layered perovskites, there is no restricted size confinement for the interlayer cations, as indicated in 3D perovskites. This structure feature allows organic cations such as butylammonium ion ($C_4H_9NH_3^+$) [55], phenylethylammonium ion ($C_8H_9NH_3^+$) [56], aromatic biimidazolium dications ($C_6H_8N_4^+$) to access to the interlayer space between inorganic layers [57]. In $(NBT)_2PbI_4$, for example, PbI_6 octahedra can link together to form a flat layer in the *bc*-plane. Instead of NBT cation, EDBE cation makes (EDBE)PbI_4 be featured as a distorted layer, that is, a <110>-oriented zigzag structure. Increasing the alkyl chain length can narrow the band gap of hybrid perovskites, which is invoked by the distortion of inorganic layers and B-I-B bond angles. Moreover, the geometrical distortion of perovskite layers can also affect the defectivity and charge relaxation dynamics. Tan et al. reported the synthesis of $(C_4H_9NH_3)_2PbBr_4$ crystals by a solution-processed method, which have a domain size of several to tens of micrometers and the thickness of several to tens of nanometers [58]. $PbBr_6$ octahedra are connected to each other via corner-sharing bromide atoms forming a 2D perovskite layer in the *bc*-plane, as shown in **Figure 4a**. Meanwhile, the space between layers is separated by $C_4H_9NH_3^+$ cations for charge balance. $(C_4H_9NH_3)_2PbBr_4$ crystal-based photodetectors assisted with the protection and electric contact of monolayer graphene was reported to exhibit very low dark current (~ 10^{-10} A),

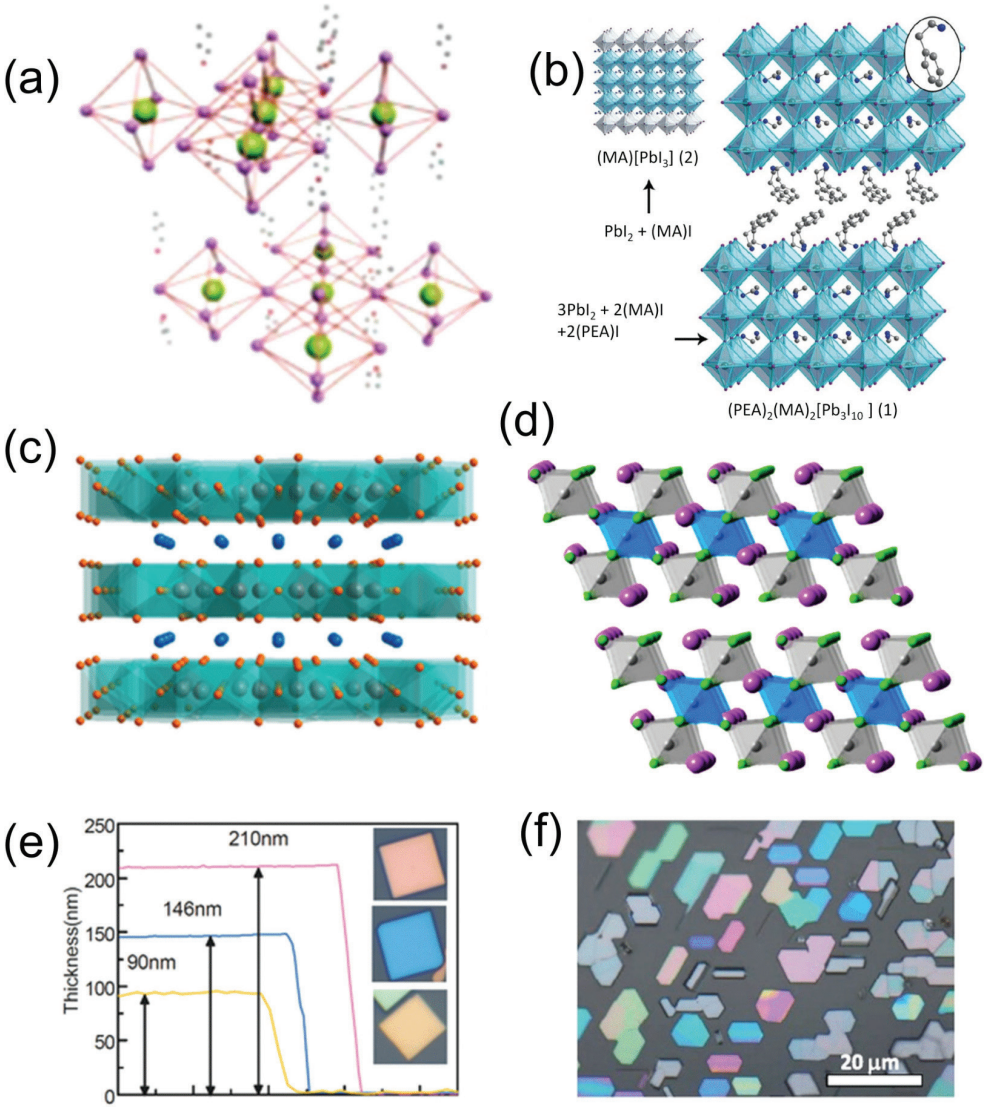

Figure 4. (a) Structural illustration of 2D layered $(C_4H_9NH_3)_2PbBr_4$ [58]. (b) 2D layered structure in $(PEA)_2(MA)_2[Pb_3I_{10}]$ [60]. (c) $[Pb_2Br_5]^-$ layer in $CsPb_2Br_5$ [62]. (d) The crystal structures of $Cs_4CuSb_2Cl_{12}$ [63]. (e) AFM characterization of individual $CsPbBr_3$ nanoplatelets with different colors [64]. (f) An optical image of $CH_3NH_3PbI_3$ nanoplatelets prepared by vapor phase method [48].

high on/off current ratio (up to 10^3) and a high responsivity of ~2100 A/W [58]. In addition, the "A" moiety can be further substituted by two types of organic cations, named as Ruddlesden-Popper family. In $(BA)_2(MA)_{n-1}Pb_nI_{3n+1}$ (n = 1, 2,3,4, ∞) perovskites, the layers are composed of tilted, corner-sharing PbI_6 octahedra, propagating in the *ac* plane, while the inorganic sheets

are disconnected by the organic bilayers. For such perovskites $(BA)_2(MA)_{n-1}Pb_nI_{3n+1}$, their band gap is 2.43 (n = 1), 2.17 (n = 2), 2.03 ((n = 3) and 1.91 (n = 4) eV, respectively [59]. If BA^+ cation is substituted with aromatic cations, such as PEA^+ cation, then resulting $(PEA)_2(MA)_2Pb_3I_{10}$ (PEA = $C_6H_5(CH_2)_2NH_3^+$, MA = $CH_3NH_3^+$) features n = 3 layers with the PEA cations sandwiched between layers and MA^+ cations situated in the layers, displaying an optical band gap of 2.06 eV (**Figure 4b**) [60].

If the inorganic framework of 3D perovskites are slit along <111> axis, <111> oriented perovskites can be obtained. Leng et al. reported a collaborative solvent- and ligand-assisted re-precipitation method for the synthesis of $MA_3Bi_2X_9$ (X = Cl, Br, I) quantum dots. $(CH_3NH_3)_3Bi_2Br_9$ has a distorted layered structure composed of corner-shared $BiBr_6$ octahedra with Cs^+ ions filled between interlayers [61]. Also, other interesting types of layered perovskite structures have been investigated. For instance, the tetragonal phase of $CsPb_2Br_5$ exhibits a sandwich structure consisting of $[Pb_2Br_5]^-$ layers and intercalated Cs^+ as shown in **Figure 4c**. In the $[Pb_2Br_5]^-$ layer, one Pb^{2+} cation coordinates with four Br^- forming the elongated pentahedron. All the Pb^{2+} ions are confined in the center of the layer, while Br^- ions are located in both the bottom and top surface of the layer. The structural feature of the $CsPb_2Br_5$ crystals is similar to that of layered double hydroxides, the nanoplatelets of which can be steadily prepared by a facile precipitation process [62]. Vargas et al. prepared a 2D inorganic metal halide perovskite single crystal of $Cs_4CuSb_2Cl_{12}$ by a solution-processed method (**Figure 4d**). They found that this perovskite has a direct bandgap of 0.98 eV obtained by DFT calculations and exhibits higher conductivity than that of $MAPbI_3$ (MA = methylammonium). Besides this, perovskite displayed high photo/thermal-stability and also tolerant to humidity, which makes it a promising candidate for optoelectronic applications [63].

As for the perovskites with a 2D morphology, Levchuk et al. reported the synthesis of $CH_3NH_3PbX_3$ (X = Br, I) nanoplatelets via a ligand-assisted re-precipitation method, tailoring the thickness of nanoplatelets between 1 and 8 unit cell monolayers [64]. Thanks to the quantum confinement effects, the thickness-dependent PL properties of these nanoplatelets would offer an effective method to tune the emission color of perovskites [64]. Vapor-phase methods have also been employed for the synthesis of 2D perovskites. CVD was used to synthesize 2D $CsPbBr_3$ nanoplatelets directly on the mica substrate via the reaction between PbX_2 and CsX (**Figure 4e**). The growth mechanism of the nanoplatelets suggested that layered mica could facilitate the VDW epitaxial growth of 3D perovskites into ultrathin 2D morphology [65]. Meanwhile, they also employed a two-step CVD procedure for the preparation of $MAPbI_3$ platelets. In this method, PbI_2 was firstly deposited on the silicon substrate, followed by the vapor-phase conversion of the PbI_2 into $MAPbI_3$ [48]. Zhang et al. reported the preparation of $CH_3NH_3PbI_{3-a}X_a$ (X = I, Br, Cl) nanoplatelets grown on muscovite mica, which showed triangular or hexagonal platelets with nanoscale thickness (10–300 nm) and edge length of several to tens of micrometers (**Figure 4f**) [66]. For a typical $CH_3NH_3PbI_3$ triangular nanoplatelet, a lasing threshold of ~37 $\mu J\ cm^{-2}$ is deduced; while for $CH_3NH_3PbI_{3-a}Br_a$ and $CH_3NH_3PbI_{3-a}Cl_a$, a higher threshold of ~128 $\mu J\ cm^{-2}$ is achieved but with a larger cavity quality factor, Q ~ 900. Integrating onto other conductive substrates such as Si, Au and ITO, respectively, the spontaneous emission lifetimes are 2.6, 1.2 and 1.9 ns. These emission times are much shorter than those on mica. However, the threshold of these nanoplatelet lasers remained to be ~40 $\mu J\ cm^{-2}$, because the exciton avalanche occurs

in a much shorter time-scale than that of the carrier transfer/trapping at the surface/interfaces. In the family of the unique perovskite nanoplatelets, they have demonstrated strong optical-pumped room-temperature near-infrared lasing with low thresholds and wide mode-tunability [66]. Liao et al. reported the single crystalline square microdisks (MDs) of $CH_3NH_3PbBr_3$ prepared by using a one-step solution self-assembly method for the first time [67]. Square MDs of $CH_3NH_3PbBr_3$ are highly emissive with PLQY = 22% ± 5%. Q value of 430 was obtained at 555 nm presented by a transverse magnetic (TM) mode, which is smaller than the simulated one. This is most likely due to the shape deformation of $CH_3NH_3PbBr_3$ MDs derivate from perfect squares. Single mode lasing at 557.5 nm was achieved in a 2.0 × 2.0 × 0.6 μm^3 square MD with a threshold of 3.6 ± 0.5 $\mu J\ cm^{-2}$. Built-in whispering-gallery mode (WGM) microresonator in single-crystalline square MDs, ambipolar charge transport and the high carrier mobility make perovskites attractive candidates to realize electrically pumped on-chip coherent light sources [67].

3.2. High-resolution characterization tools

Grazing incidence wide angle X-ray scattering (GIWAXS) has been widely used to evaluate the lattice expansion in perovskite materials. As shown in **Figure 5a**, the *d* spacing of relative peaks is larger than that of the bulk crystals, consistent with the transmission electron microscopy (TEM) measurements of single sheets [68].

Atomic force microscopy (AFM) measurements are usually employed to detect the thickness and surface of perovskite nanosheets and nanoplatelets. Yang et al. reported that the thickness of 2D $(PEA)_2PbI_4$ NSs is measured as 2.0 ± 0.1 nm by AFM (**Figure 5b**), showing the formation of single-layer nanosheets [69]. According to the crystallographic model, the theoretical interlayer distance should be 1.64 nm. Thus, it is very close to the AFM results, given the fact that some organic molecules adsorbed on the surface of perovskite nanosheets. Besides, a quite smooth surface of the $(PEA)_2PbI_4$ nanosheet was observed from the high-magnification height profile (right, **Figure 5b**).

Transmission electron microscopy (TEM), high-resolution TEM (HRTEM) and high-angle annular dark-field scanning TEM (HAADF-STEM) are all-powerful tools for analysis of 2D perovskite structures. Akkerman et al. reported the face-to-face alignment of $CsPbBr_3$ nanoplatelets with a thickness of 3.0 ± 0.4 nm (corresponding to 5 unit cells) and the average lateral dimensions of 7.9 ± 1.2 nm × 40.9 ± 6.8 nm (**Figure 5c**). HRTEM images confirmed that $CsPbBr_3$ nanoplatelets are lying flat with respect to the substrate (**Figure 5d**). And the high crystallographic structure of these nanoplatelets can be well characterized by Fast Fourier Transform (FFT) images (**Figure 5e**) [70]. In the STEM mode, these nanoplatelets are lying flat or edge-on on the substrate (**Figure 5f**).

Single crystal X-ray diffraction is another powerful technique to analyze the structure of new materials by collecting diffraction data on single crystals. Recently, Cortecchia et al. found that a significant deformation of the Pb − X bond length and the X − Pb − X bond angle can result in broadened PL spectra for the two perovskites, $(NBT)_2PbI_4$ [71] and $(EDBE)PbI_4$ [72] (NBT = n-butylammonium and EDBE = 2,2-(ethylenedioxy)bis(ethylammonium)) [73].

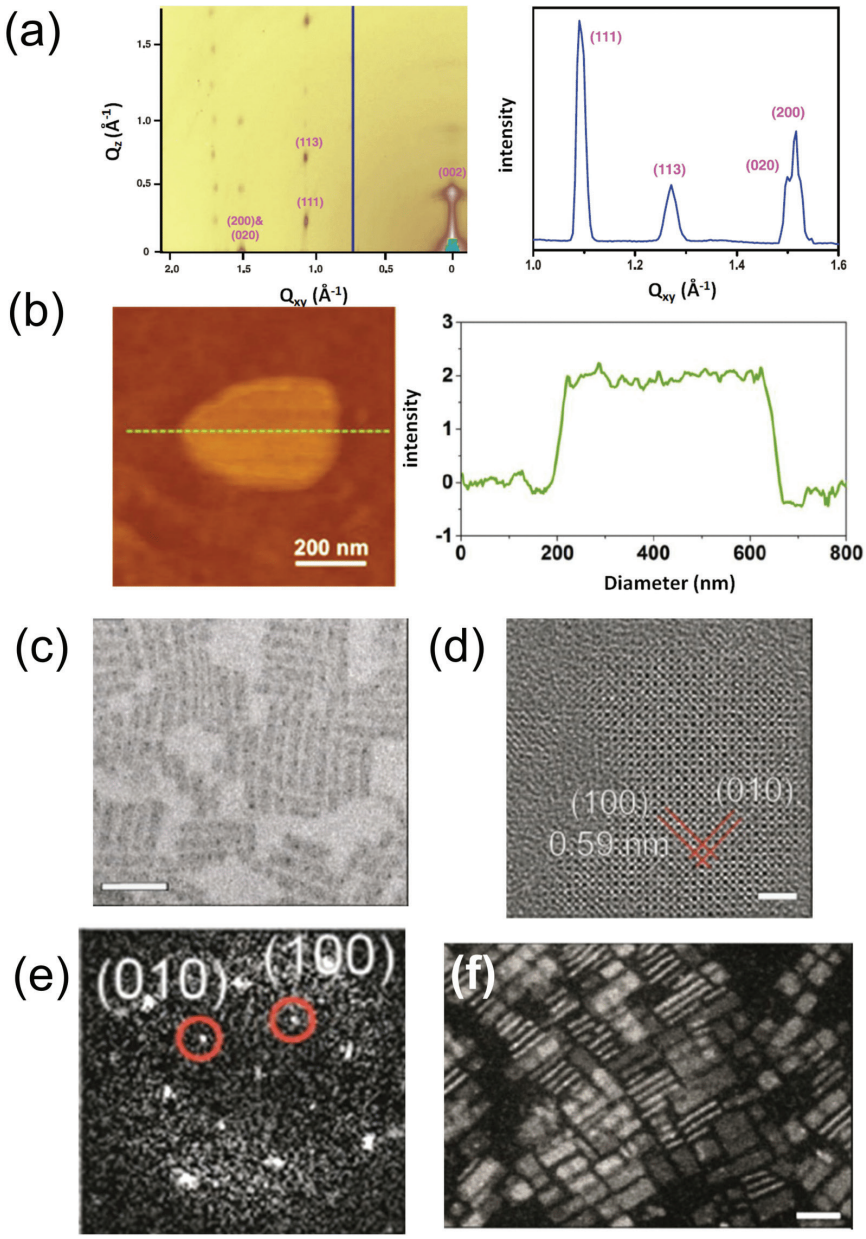

Figure 5. (a) GIWAXS image of the 2D thin sheets (left) and integrated GIWAXS spectrum of the 2D thin sheets (right) [68]. (b) AFM image (left) and height profile (right) of a typical $(PEA)_2PbI_4$ nanosheet synthesized in toluene [69]. (c) TEM, (d) HRTEM and (e) FFT images of $CsPbBr_3$ NPLs. (f) STEM dark-field image of $CsPbBr_3$ nanoplatelets [70]. Scale bars correspond to 50 nm in (c), 2 nm in (d) and 20 nm in (f).

4. Applications of 2D perovskites as photodetector materials

Responsivity, speed and sensitivity are three main factors for evaluating photodetectors. Responsivity is the ratio of photocurrent/photovoltage to the incident optical power, $R = I_{out}/P_{in}$. Speed is derived from the rise and fall response times, respectively, of a transient photocurrent. Sensitivity measures the ability to detect a weak light signal and is reported as the specific detectivity, $D^* = R\ (A \cdot \Delta f)1/2\ I_{noise}^{-1}$. Devices with a high responsivity and a small noise current can achieve a signal-to-noise ratio of 1, which corresponds to the noise-equivalent intensity (i.e. the detection limit) at a lower incident intensity. Specific detectivity is normalized to the device area and the frequency bandwidth of the noise measurement, enabling comparison among different device architectures, areas and measurement bandwidths.

There are three kinds of photodetectors: *photoconductors*, *phtototransistors* and *photodiodes*. Charge carriers in photoconductors are re-circulated through symmetrical contacts, in which an external voltage is applied to read out the photon-derived changes and to achieve gains through multiple carrier re-circulation. In contrast to photoconductors, a built-in potential in a junction of photodiodes is essential for extraction of the photo-generated carriers. In phototransistors, a gate-programmable semiconducting channel is optoelectronically modulated, which might assist or hinder the charge transport while providing gain.

In this section, applications of 2D layered perovskites and perovskite nanoplatelets or nanosheets as the key component in fabrication of photodetectors are summarized and discussed.

4.1. Photodetectors based on 2D layered perovskites

Compared to perovskite film-based photodetectors, photodetectors made of perovskite single crystals exhibit more efficient photoresponsivity. In 2016, Tan *et al.* reported a solution-processed synthesis of $(C_4H_9NH_3)_2PbBr_4$ crystals on SiO_2/Si substrates under room temperature and application in the fabrication of photodetectors [58]. Individual 2D perovskite crystal-based photodetectors were constructed along with large-area monolayer single-crystal graphene film used as a protection layer from dissolution into water or acetone, which has improved the stability of this device (**Figure 6a**). More importantly, water was carefully excluded during the transfer of graphene onto the perovskite crystals through a special "dry" transfer method. Interdigital graphene electrodes were designed to improve the absorption cross section of 2D perovskite crystals (**Figure 6b**). Finally, the photodetector displayed an ultrahigh photoresponsivity up to 2100 A/W and an On/Off ratio of 10^3 (**Figure 6c** and **d**). Such an efficient photoresponse is most likely attributed to the strong adsorption of 2D perovskite crystals on and enhanced carrier collection by graphene electrodes. This report represents the first time to fabricate a novel photodetector based on 2D individual perovskite crystals combining graphene-based source-drain electrodes, and the results could open a new avenue for the development perovskite crystals based optoelectronic devices [58].

Zhou et al. reported the synthesis of three different 2D layered structures, $(C_4H_9NH_3)_2PbI_4$ (n = 1, one-layered perovskite), $(C_4H_9NH_3)_2(CH_3NH_3)Pb_2I_7$ (n = 2, two-layered perovskite) and $(C_4H_9NH_3)_2(CH_3NH_3)_2Pb_3I_{10}$ (n = 3, three layered perovskite) [74]. Especially, the photodetector based on three-layered perovskite displayed higher I_{light}/I_{dark} ratio on the order of ~10^3

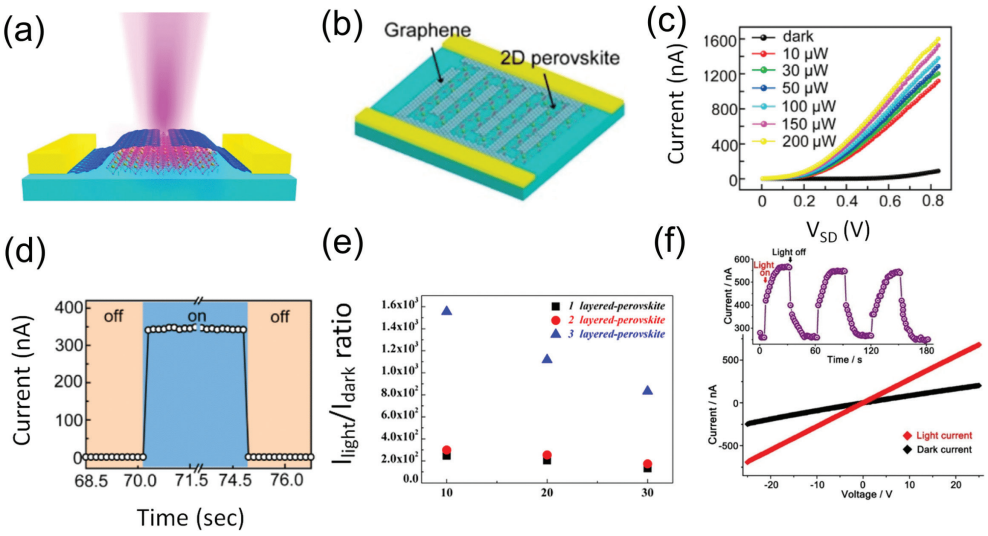

Figure 6. Schematic illustration of the structure of 2D $(C_4H_9NH_3)_2PbBr_4$-based photodetector with (a) single-crystalline graphene film connecting the source-drain top electrodes [58] and (b) interdigital graphene electrodes [58]. (c) Current-voltage curves obtained in the dark and under different illumination intensity using a 470 nm defocused laser [58]. (d) Transient photocurrent recorded [58]. (e) Dependence of I_{light}/I_{dark} ratio on applied voltage [74]. (f) Photocurrents generated by a pellet of $(TMP)_{1.5}[Bi_2I_7Cl_2]$ [75].

(**Figure 6e**). However, compared to 3D perovskites, these photodetectors showed much lower responsivities, which can be attributed to their larger optical band gap, small absorption in the UV-vis absorption spectrum as well as the limitation of charge carrier mobility from the insulting butylammonium layers. Among three photodetectors, three-layered photodetector displayed better performance than the others did. The reason might be that it has a narrow band gap and its microstructure is favorable to achieve higher output current.

More recently, the first 2D and mixed-halide anion of bismuth was synthesized by Li et al. via solution-processed method [75]. In this compound, a unique 2D honeycomb-like $[Bi_2I_7Cl_2]_n^{3n-}$ layers are isolated by TMP^{2+} cations (N,N,N′,N′-tetramethylpiperazine). The bandgap of this material is 2.10 eV according to optical measurements. For the electrical conductivities, pellets and single crystal of $(TMP)_{1.5}[Bi_2I_7Cl_2]$ displayed higher conductivity of 1.59×10^{-6} S/cm and 2.37×10^{-6} S/cm, respectively. Under the illumination of 450 W Xenon lamp and external applied voltage of 25 V, the photocurrent increased to 0.68 μA (**Figure 6f**). Furthermore, no material decomposition was observed after stored in air for 1 week, showing superior stability over commonly used $APbI_3$ [75].

4.2. Photodetectors using 2D perovskite nanoplatelets or nanosheets

Song et al. first reported the fabrication of atomically thin, 2D $CsPbBr_3$ nanosheets on ITO/PET substrates as a flexible and ultrathin photodetector via centrifugal casting method (**Figure 7a**) [76]. $CsPbBr_3$ nanosheets were synthesized with a thickness of ~3.3 nm and an edge length of ~1 μm, and

their typical shape is tetragonal. In contrast to organometallic halide perovskites, the as-prepared $CsPbBr_3$ nanosheets are well dispersible in several organic solvents. UV–vis absorption spectra indicated a favorable absorption capability with a direct bandgap of ~2.32 eV for the nanosheets.

Linear and symmetrical photocurrent plots further evidenced the uniform dispersion of perovskite nanosheets on the ITO electrode [76]. A high light on/off ratio of $>10^3$ under 442 nm laser was demonstrated, showing good light-switching behavior. And a peak value of 0.25 A W^{-1} was obtained under 5 V at 517 nm, as shown in **Figure 7b**, comparable to that of commercial Si photodetectors (< 0.2 A W^{-1}). Besides, external quantum efficiency (EQE) was measured to be 53% at 515 nm and 10 V bias voltage (**Figure 7c**). The rise and decay time of the $CsPbBr_3$

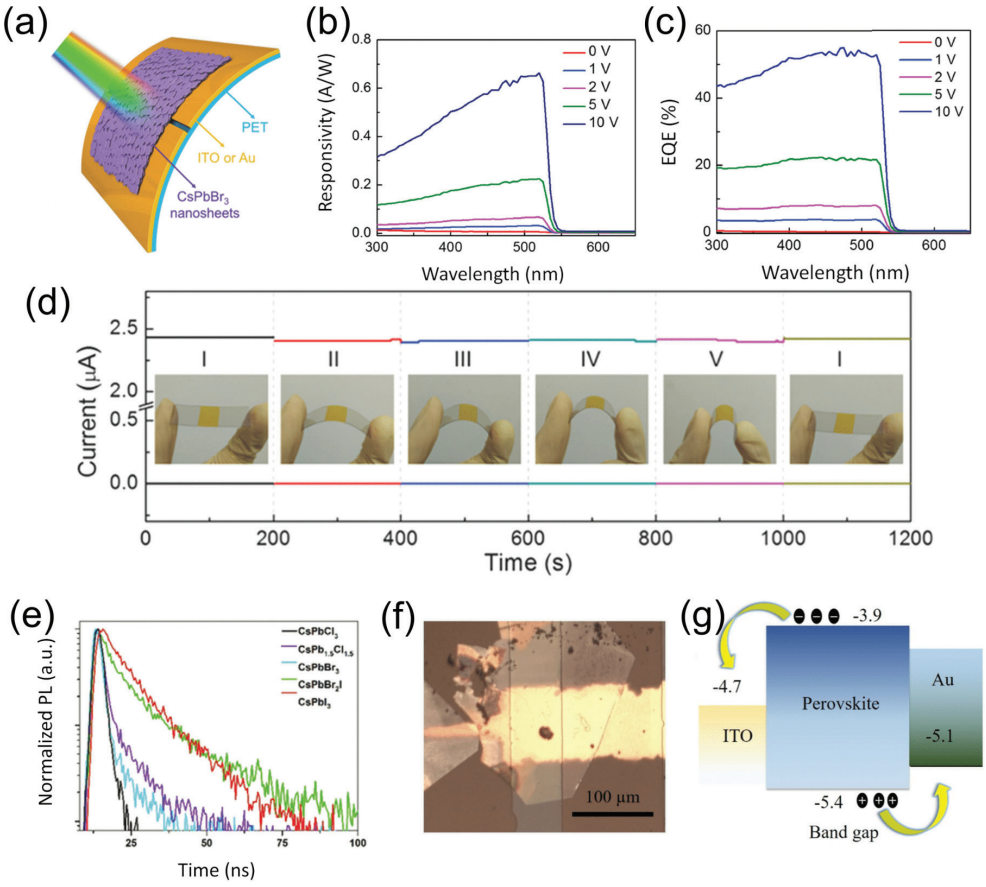

Figure 7. (a) Schematic diagram of the photodetector structure based on $CsPbBr_3$ nanosheets [76]. (b) Responsivity [76] and (c) EQE curves of $CsPbBr_3$ nanosheets based photodetectors under different forward biases [76]. (d) I–t curves of the flexible photodetector at different bending states with an applied bias voltage of 5.0 V. The insets show corresponding photographs of the device under the different bending states [76]. (e) Time-resolved PL decay transient spectra for $CsPbBr_3$ nanosheet thin films [76]. (f) Optical microscopic image of the device structure for the $CH_3NH_3PbI_3$ vertical-type photodetector [78]. (g) The band alignment for the ITO/perovskite/Au vertical heterostructure [79].

Device component and structure	Perovskite structure	Rise-decay time (ms)	On/off ratio	Responsivity (A W^{-1})	Ref.
Au/$(C_4H_9NH_3)_2PbBr_4$/graphene	Single crystal	–	10^3	2100	[58]
Glass/$(C_4H_9NH_3)_2PbI_4$/Au	Nanocrystal	28.4/27.5	1×10^2	3.00	[74]
Glass/$(C_4H_9NH_3)_2(CH_3NH_3)Pb_2I_7$/Au	Nanocrystal	8.4/7.5	1×10^2	7.31	[74]
Glass/$(C_4H_9NH_3)_2PbI_4$/Au	Nanocrystal	10.0/7.5	1×10^3	12.78	[74]
Pt/$(TMP)_{1.5}[Bi_2I_7Cl_2]$/Pt	Single crystal	–	3.4	–	[75]
ITO/$CsPbBr_3$/ITO	Nanosheet	0.019/0.024	$> 10^4$	0.64	[76]
Si/SiO_2/$CH_3NH_3PbI_3$/Ti/Au	Nanosheet	–	1×10^2	22	[77]
Au/$CsPbBr_3$/Au	Nanosheet	14.7/15.2	1×10^2	–	[78]
ITO/$CH_3NH_3PbI_3$/Au	Nanosheet	320/330	–	0.036	[79]
Au/$CH_3NH_3PbI_3$/Au	Nanosheet	230/190	–	–	[79]

Table 1. Comparison of the performances of 2D perovskites-based photodetectors.

photodetector were 19 and 25 μs, respectively. Meanwhile, the photodetectors were resistant to external bending stress as the photocurrents and dark currents remained unchanged at different bending states (**Figure 7d**). Also, after bending and recovering for >1000 times, the photodetector still showed high light on/off ratio, showing very high stability. In contrast to serious degradation of $MAPbBr_3$ photodetectors, $CsPbBr_3$ nanosheet photodetector almost remained unchanged under ambient environment. These results open up the opportunity for the practical application of 2D perovskite materials used as photodetectors due to their high stability [76]. In another example, Liu et al. reported a combined solution processing and vapor-phase conversion method to synthesize $CH_3NH_3PbI_3$ nanosheets as thin as a single unit cell (~ 1.3 nm), which were used in fabrication of a field-effect transistor [77]. This device displayed enhanced photocurrent upon illumination as well as high ratio of photocurrent to dark current, attributing to strong light-matter interaction and broad-band light-harvesting capability in a single-unit-cell nanosheet. Under illumination of a 405 nm laser, photoresponsivity can reach 22 A W^{-1}. Besides, the rise and decay time of the photodetector shorter than 20 and 40 ms exhibited a much faster response time than bulk films, showing potential application for optoelectronic switches and photodetectors.

Cyan-emitting $CsPbBr_3$ nanosheets based photodetector was reported by Lv et al. [78]. The source-drain current of $CsPbBr_3$ nanosheet film in the dark was detected to be on the order of 10^{-12} A due to the existence of long-chain organic ligands on the nanosheet surface. Under illumination of a laser diode at 450 nm, a significant increase in photocurrents was observed. Besides, excellent optical switching and stability of this photodetector were also proved under 1 Hz pulse laser (450 nm) at a fixed light density of 13 mW cm^{-2} with a bias voltage of 1 V. Through fitting the photocurrent response curve (**Figure 7e**), the rise time was estimated to be 17.8 ms and the decay times were determined to be 14.7 and 15.2 ms [78]. Li et al. used a combined solution-processed and vapor-phase conversion method for the synthesis of 2D $CH_3NH_3PbI_3$ nanosheets with a thickness of ~20 nm [79]. Vertical- and planar-type photodetectors based on $CH_3NH_3PbI_3$

nanosheets were tested to evaluate their optoelectronic properties (**Figure 7f**). With increasing the incident laser power, the photocurrent increased to 600 nA at the power of 98.56 μW. The rise and decay times of the photodetector were measured to be 320 and 330 ms, respectively. Comparable to planar-type photodetector, the vertical-type photodetector displayed higher photoresponsivity, about 36 mA W^{-1} under excitation power of 50.82 μW, resulting from short transmission distance of the photocarriers between the electrodes in the vertical photodetector and appropriate band energy distribution (**Figure 7g**). All these results might open a new avenue for the investigation of 2D perovskites including their optical, electronic and optoelectronic properties and for potential application as practical photodetectors.

Other photodetectors based on 2D halide perovskites have also been reported. **Table 1** compares the structure and key performance parameters of recently reported photodetectors.

5. Theoretical analysis and simulations

First-principles calculations based on density functional theory (DFT) have been used to simulate the electronic structures of many body systems from atomic level quantum mechanics. Recently, perovskite-based materials including lead-free perovskites, 3D perovskites, especially 2D perovskites have been studied using first-principles calculations, exploring their electron/hole effective masses, band gaps, carrier mobility, theoretical absorption spectra and other properties related to their potential applications. Besides DFT calculations, the local density approximation (LDA) and the generalized gradient approximation (GGA) functional have also been used in many systems due to their simplicity. However, these two methods usually underestimate band gaps of solids by 30–100%. Therefore, Green-function approximation (GWA) [80], time-dependent DFT (TDDFT), [81] HSE06, [82] and PBE0 hybrid functionals, [83] and more recent Delta self-consistent-field method [84] were mainly employed in theoretical calculations of perovskites. Spin-orbit coupling (SOC) is required to be included in calculations with the presence of heavy atoms to achieve a more accurate prediction of electronic structures.

For lead-free peroskites, first-principles quantum mechanical calculations were used to investigate their thermodynamic stability and photovoltaic-related properties. To this end, a series of design metrics including thermodynamic and crystallographic stability, light absorption, carrier effective mass, dopability, exciton binding and others should be considered [85]. For example, the latest calculations have identified 18 compounds out of ~100 possible candidates as most-likely targets (**Figure 8a**). Furthermore, the structure-property relationship was also studied and showed that changes in microscopic structures could significantly affect photovoltaic performance. Theoretical computations could serve as a roadmap for facilitating experimental discovery of alternative solar-energy hybrid perovskites. Sn- and Ge-based alternatives were reported to be more stable than Pb-based perovskites. However, they displayed poor performance in solar cells largely because of their intrinsic p-type conductivity and decrease in photocurrent density, and fill factor. Therefore, other factors beyond intrinsic bulk properties should be included in order to evaluate their performance more reliably.

Using DFT the electronic band structure and density of states of some 2D perovskites were computed, which confirmed that these 2D perovskites are indeed direct band gap semiconductors.

Their valence band mostly consists of I 5p states with a small amount of Pb 6 s, while their conduction band primarily consists of Pb 6p states. For example, the band gap is 1.99 eV for $(BA)_2PbI_4$, 1.78 eV for $(BA)_2(MA)_2Pb_3I_{10}$ and 0.96 eV for $(BA)_2(MA)_3Pb_4I_{13}$ (**Figure 8b** and **c**), respectively. It is found that the band gap decreases with increasing the number of perovskite layers. Besides, the structural stability of these materials was predicted by DFT, finding that non-centrosymmetric structures in 2D perovskites with a large number of layers are favorable. However, there is still a complex relationship between the perovskite layer thickness and lateral dimension [59]. Akkerman et al. reported the SOC-DFT calculations to investigate the electronic properties of $CsPbBr_3$ NPLs (**Figure 8d**), which is highly consistent with the experimentally observed band-gap evolution [70]. SOC effects can determine electronic and optical properties of perovskites as well as their quantum confinement behavior. However, deviations become obvious as the quantum wells decreased to ultrasmall dimension. This is mainly attributed to the tunneling of the electron/hole wave functions outside the well boundaries such as the lack of effectively

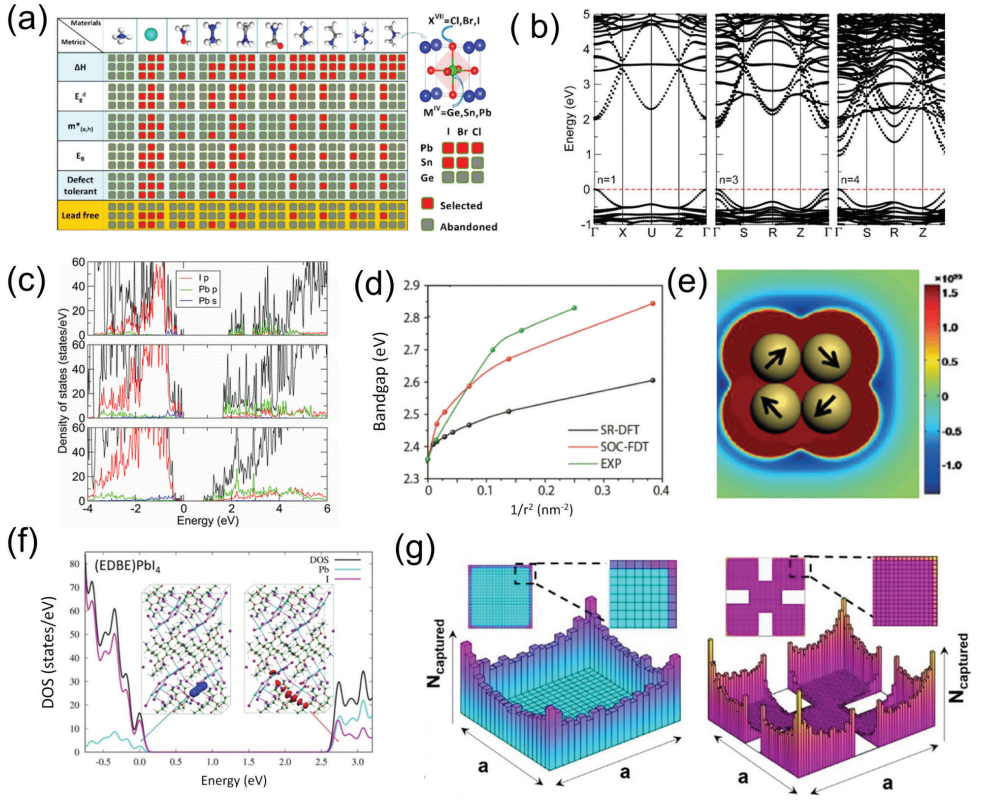

Figure 8. (a) Screening process for the potential superior bulk-material-intrinsic photovoltaic performance by first-principle calculations [85]. (b) Electronic band structure [59] and (c) DOS results of the polar configurations in $(BA)_2(MA)_{n-1}Pb_nI_{3n+1}$ [59]. (d) Band gaps from experiment and SR-, SOC-DFT calculations [70]. (e) Simulations of total potential field in a four-dot alignment [53]. (f) DOS curves of the neutral lead vacancy and isodensity plot of the defect states in $(EDBE)PbI_4$ [73]. (g) 3D bar charts showing Monte Carlo simulation results for a square (left) and fractal (right) seeds [50].

infinite potential barriers at the NPL border. In addition, the effective masses and the exciton both reduced with increasing quantum confinement, suggesting ambipolar transport occurred in $CsPbBr_3$ crystals.

To better understand the self-organization mechanisms of $CH_3NH_3PbBr_3$ QDs (or nanodots (NDs)) into NPLs, Liu et al. performed theoretical simulations based on the classical Derjaguin-Landau-Verwey-Overbeek (DLVO) theory [53]. They suggested that during the self-organization process, two or four coalescent QDs might be considered as stable units. Two coalescent QDs attracted each other from bottom and top to form a four-dot alignment under dipole-dipole attraction (**Figure 8e**). With a combination of VDW and electrostatic driving forces, the self-organization of $CH_3NH_3PbBr_3$ QDs preferred via side-side orientation to form nanoplatelets. Consequently, the axis size of NPLs is about four-fold that of building block QDs.

Cortecchia et al. have performed ab initio calculations to investigate the structural effects on the defectivity and energetic landscape for $(EDBE)PbI_4$. For the neutral Pb vacancy, formation of I_3^- trimer is preferred in $(EDBE)PbI_4$ by ~1 eV, which is driven by under-coordinated iodine atoms at the organic/inorganic interface with partial charge stabilized by $EDBE^{2+}$ [73]. However, iodine atoms per organic cation in $(NBT)_2PbI_4$ has a stronger electrostatic interaction, which prevents the vicinal iodine motion from forming I_3^-. Hybrid DFT calculations including spin-orbit coupling (PBE0-SOC) was also conducted to verify the formation of I_3^- trimer in $(EDBE)PbI_4$ (**Figure 8f**). An optical transition at 0.21 eV corresponds to the highest occupied molecular orbital (HOMO)-Lowest unoccupied molecular orbital (LUMO) transition of I_3^-, leading to the emergence of Stokes-shifted, broadened luminescence according to the relaxation mechanism for trapped charge carriers. With the templating cation assisting charge localization, the increased structural distortions in the PbX_6 octahedral coordination in $(EDBE)PbI_4$ lower the energy barrier for self-trapping and thus stabilize the trimer I_3^-.

In addition, Monte Carlo calculations were used to explain the growth mechanism of 2D sheets of $MAPbCl_3$ on mica [50]. The VDW nucleation and growth model was proposed (**Figure 8g**) [50]. The competition between the VDW diffusion and cohesive energy of perovskites can in principle increase the thickness of perovskite sheets. This means much thicker layered perovskites could be prepared through surface passivation. Furthermore, the development of two-photon-pumped laser combined theoretical simulations (e.g. two-photon absorption (TPA)) would enable to study certain perovskites towards understanding their nonlinear optical properties. For example, Chen et al. have recently revealed that the TPA process proceeds through a virtual level and then ended in an exciton band state. This observation would lay a solid physic basis for the development of high-performance nonlinear optical perovskite materials [86].

6. Concluding remarks and outlook

Metal halide perovskites have increasingly attracted research interests in recent years, largely because of their remarkable optical and electronic properties such as high carrier mobility, small exciton binding energy, high photoluminescence quantum yield, narrow bandwidth, long charge diffusion length and broadly tunable bandgap. They can further exhibit unique

http://dx.doi.org/10.5772/intechopen.71032

optical properties and enhanced stability in their 2D form due to quantum confinement effects, which has led to increasing interest in the design and assembly of 2D perovskites for their applications in photodetectors. This chapter mainly focused on the introduction of synthesis methods, structure characterizations for both 2D layered perovskites and 2D perovskites in shape, along with summarizing photodetection application of these two types of 2D perovskites.

Researchers have made tremendous progress in studying 2D perovskite-based photodetection techniques, but some challenges from both basic science and device engineering perspective remain to be overcome. Recent studies have shown the feasibility of preparation of perovskite nanosheets and nanoplatelets, but the control of their morphology and thickness needs to be improved. Due to the quantum confinement effects, the thickness of nanoplatelets or nanosheets is a critical factor for their optical properties. Therefore, the development of improved synthetic methods for better controlling morphology and thickness are indeed required, which has been well achieved in conventional semiconductors and metal nanocrystals. With the development of two-photon-pumped laser for studying $CsPbBr_3$ QDs, the nonlinear optical properties of perovskites have just been taken to the front of the research, such as two-photon absorption (TPA). Although 2D metal halide perovskites have displayed excellent optical properties, water and air stability is still a detrimental problem towards their practical applications. Some recent researches have attempted to solve this issue. For example, organic molecular capping, silica or Al_2O_3 coatings were used to improve the stability, which has been to some extent successful. However, further efforts still need to find more general ways with broad suitability for 2D perovskites. Meanwhile, another important issue, similar to stability, is the toxicity of Pb element, which is one of the most insidious factors for the environment and human. Albeit with the excellent properties of lead-containing 2D perovskites, it still exposes as a detriment factor for their applications. Many attempts have been made to substitute Pb with nontoxic metal elements, but the resulting perovskites normally do not have the same level performance. For example, Sn-based perovskites have appropriate bandgaps for optoelectronic applications, but they display much lower stability than Pb-containing perovskites due to the oxidation of Sn^{2+} to Sn^{4+} under ambient conditions. For Ge- and Bi-based perovskites, they indeed display high stability. However, these two types of perovskites possess a large bandgap, which limits the light absorption in long-wavelength range. Therefore, it is high desirable to design new 2D layered perovskites with appropriate bandgap and large absorption coefficient and high stability.

In terms of photodetection applications, being comparable to conventional colloidal quantum-dot-based photodetectors much improvement is needed for perovskites. For example, perovskite-based photoconductors suffer from slow photoresponse, low sensitivity and large electrical hysteresis. Some recent efforts have partially overcome these issues by using surface passivation, phototransistor gating and fabricating hybrid bilayer photodetectors. Interfacing perovskite layers with other functional nanomaterials is proposed to be an effective way for fabricating perovskite-based optoelectronic devices. In a broader perspective, perovskite-based materials could be tuned and engineered for fabrication of new-type devices that are endowed with new functions such as multi-spectral sensing.

In conclusion, in view of their novel structures and optical properties we would believe that 2D perovskites are on the way becoming promising materials for next-generation optoelectronic devices.

Acknowledgements

This work was supported by Independent Research Fund Denmark-Nature Sciences (DFF-FNU, to Q.C.) and the Villum Foundation (to Q.C. and Y.T.). Y.T. is grateful for the Villum Foundation supported postdoc fellowship. X.C. is grateful for the support from the Chinese Scholarship Council (PhD scholarship No. 201406170040).

Author details

Yingying Tang, Xianyi Cao and Qijin Chi*

*Address all correspondence to: cq@kemi.dtu.dk

Department of Chemistry, Technical University of Denmark, Kongens Lyngby, Denmark

References

[1] Büchele P, Richter M, Tedde SF, Matt GJ, Ankah GN, Fischer R, Biele M, Metzger W, Lilliu S, Bikondoa O, Macdonald JE, Brabec CJ, Kraus T, Lemmer U, Schmidt O. X-ray imaging with scintillator-sensitized hybrid organic photodetectors. Nature Photonics. 2015;**9**:843-848. DOI: 10.1038/nphoton.2015.216

[2] Huang SM, Huang SJ, Yan YJ, SH Y, Chou M, Yang HW, Chang YS, Chen RS. Extremely high-performance visible light photodetector in the Sb_2SeTe_2 nanoflake. Scientific Reports. 2017;**7**:45413. DOI: 10.1038/srep45413

[3] Sobhani A, Knight MW, Wang YM, Zheng B, King NS, Brown LV, Fang ZY, Nordlander P, Halas NJ. Narrowband photodetection in the near-infrared with a plasmon-induced hot electron device. Nature Communications. 2013;**4**:1643. DOI: 10.1038/ncomms2642

[4] Karim A, Andersson JY. Infrared detectors: Advances, challenges and new technologies. IOP Conference Series: Materials Science and Engineering. 2013;**51**:012001. DOI: 10.1088/1757-899X/51/1/012001

[5] Jansen-van Vuuren RD, Pivrikas A, Pandey AK, Burn PL. Colour selective organic photodetectors utilizing ketocyanine-cored dendrimers. Journal of Materials Chemistry C. 2013;**1**:3532-3543. DOI: 10.1039/C3TC30472H

[6] Ko WS, Bhattacharya I, Tran TTD, Ng KW, Gerke SA, Chang-Hasnain C. Ultrahigh responsivity-bandwidth product in a compact InP nanopillar phototransistor directly grown on silicon. Scientific Reports. 2016;**6**:33368. DOI: 10.1038/srep33368

[7] Mokkapati S, Jagadish C. III-V compound SC for optoelectronic devices. Materials Today. 2009;**12**:22-32. DOI: 10.1016/S1369-7021(09)70110-5

[8] de Arquer PGF, Armin A, Meredith P, Sargent EH. Solution-processed semiconductors for next-generation photodetectors. Nature Reviews Materials. 2017;**2**:16100. DOI: 10.1038/natrevmats.2016.100

[9] McNeill R, Siudak R, Wardlaw J, Weiss D. Electronic conduction in polymers. I. The chemical structure of polypyrrole. Australian Journal of Chemistry. 1963;**16**:1056-1075. DOI: 10.1071/CH9631056

[10] Coffey DC, Ferguson AJ, Kopidakis N, Rumbles G. Photovoltaic charge generation in organic semiconductors based on long-range energy transfer. ACS Nano. 2010;**4**:5437-5445. DOI: 10.1021/nn101106b

[11] Huang J, Miragliotta J, Becknell A, Katz HE. Hydroxy-terminated organic semiconductor-based field-effect transistors for phosphonate vapor detection. Journal of the American Chemical Society. 2007;**129**:9366-9376. DOI: 10.1021/ja068964z

[12] Nath D, Dey P, Deb D, Rakshit JK, Roy JN. Fabrication and characterization of organic semiconductor based photodetector for optical communication. CSI Transactions on ICT. 2017;**5**:149-160. DOI: 10.1007/s40012-016-0150-8

[13] Guo YL, Liu C, Tanaka H, Nakamura E. Air-stable and solution-processable perovskite photodetectors for solar-blind UV and visible light. The Journal of Physical Chemistry Letters. 2015;**6**:535-539. DOI: 10.1021/jz502717g

[14] Pei YL, Pei RH, Liang XC, Wang YH, Liu L, Chen HB, Liang J. CdS-nanowires flexible photo-detector with Ag-nanowires electrode based on non-transfer process. Scientific Reports. 2016;**6**:21551. DOI: 10.1038/srep21551

[15] Oertel DC, Bawendia MG. Photodetectors based on treated CdSe quantum-dot films. Applied Physics Letters. 2005;**87**:213505. DOI: 10.1063/1.2136227

[16] Mi LF, YQ Y, Wang H, Zhang Y, Yao XD, Chang YJ, Wang XM, Jiang Y. Ultrasensitive PbS-quantum-dot photodetectors for visible–near-infrared light through surface atomic-ligand exchange. Particle & Particle Systems Characterization. 2015;**32**:1102-1109. DOI: 10.1002/ppsc.201500138

[17] Zhou YY, Zhu K. Perovskite solar cells shine in the "Valley of the Sun". ACS Energy Letter. 2016;**1**:64-67. DOI: 10.1021/acsenergylett.6b00069

[18] Congreve DN, Weidman MC, Seitz M, Paritmongkol W, Dahod NS, Tisdale WA. Tunable light-emitting diodes utilizing quantum-confined layered perovskite emitters. ACS Photonics. 2017;**4**:476-481. DOI: 10.1021/acsphotonics.6b00963

[19] Sutherland BR, Johnston AK, Ip AH, JX X, Adinolfi V, Kanjanaboos P, Sargent EH. Sensitive, fast, and stable perovskite photodetectors exploiting interface engineering. ACS Photonics. 2015;**2**:1117-1123. DOI: 10.1021/acsphotonics.5b00164

[20] Wolf SD, Holovsky J, Moon SJ, Löper P, Niesen B, Ledinsky M, Haug FJ, Yum JH, Ballif C. Organometallic halide perovskites: Sharp optical absorption edge and its relation to photovoltaic performance. The Journal of Physical Chemistry Letters. 2014;**5**:1035-1039. DOI: 10.1021/jz500279b

[21] Du Y, Cai H, Wu Y, Xing Z, Li Z, Xu J, Huang L, Ni J, Li J, Zhang J. Enhanced planar perovskite solar cells with efficiency exceeding 16% via reducing the oxygen vacancy defect state in titanium oxide electrode. Physical Chemistry Chemical Physics. 2017;**19**:13679-13686. DOI: 10.1039/c7cp01936j

[22] Guo Z, Manser JS, Wan Y, Kamat PV, Huang LB. Spatial and temporal imaging of long-range charge transport in perovskite thin films by ultrafast microscopy. Nature Communications. 2015;**6**:7471. DOI: 10.1038/ncomms8471

[23] Wang YC, Zhang YM, Liu YT, Pang TQ, ZY H, Zhu YJ, Luan SZ, Jia RX. Temperature-dependence studies of organolead halide perovskite-based metal/semiconductor/metal photodetectors. RSC Advances. 2017;**7**:20206-20211. DOI: 10.1039/C7RA01496A

[24] Su L, Zhao ZX, Li HY, Yuan J, Wang ZL, Cao GZ, Zhu G. High-performance organolead halide perovskite-based self-powered triboelectric photodetector. ACS Nano. 2015;**9**:11310-11316. DOI: 10.1021/acsnano.5b04995

[25] Zhao FY, Xu K, Luo X, Lv WL, Peng YQ, Wang Y, Lu FP, Xu SN. Ultrasensitivity broadband photodetectors based on perovskite: Research on film crystallization and electrode optimization. Organic Electronics. 2017;**46**:35-43. DOI: 10.1016/j.orgel.2017.03.023

[26] Park Y, Lee S, Park HJ, Baac HW, Yoo G, Heo J. Hybrid metal-halide perovskite-MoS_2 phototransistor. Journal of Nanoscience and Nanotechnology. 2016;**16**:11722-11726. DOI: 10.1166/jnn.2016.13581

[27] Nam KT, Shelby SA, Choi PH, Marciel AB, Chen R, Tan L, Chu TK, Mesch RA, Lee BC, Connolly MD, Kisielowski C, Zuckermann RN. Free-floating ultrathin two-dimensional crystals from sequence-specific peptoid polymers. Nature Materials. 2010;**9**:454-460. DOI: 10.1038/nmat2742

[28] Zhang H. Ultrathin two-dimensional nanomaterials. ACS Nano. 2015;**9**:9451-9469. DOI: 10.1021/acsnano.5b05040

[29] Lin Z, Carvalho BR, Kahn E, Lv RT, Rao R, Terrones H, Pimenta MA, Terrones M. Defect engineering of two-dimensional transition metal dichalcogenides. 2D Mater. 2016;**3**:022002. DOI: 10.1088/2053-1583/3/2/022002

[30] Cai SL, Zhang WG, Zuckermann RN, Li ZT, Zhao X, Liu Y. The organic flatland-recent advances in synthetic 2D organic layers. Advanced Materials. 2015;**27**:5762-5770. DOI: 10.1002/adma.201500124

[31] Stine R, Lee WK, WhitenerJr KE, Robinson JT, Sheehan PE. Chemical stability of graphene fluoride produced by exposure to XeF_2. Nano Letter. 2013;**13**:4311-4316. DOI: 10.1021/nl4021039

[32] Luan VH, Tien HN, Hoa LT, Hien NTM, Oh ES, Chung JS, Kim EJ, Choi WM, Kong BS, Hur SH. Synthesis of a highly conductive and large surface area graphene oxide hydrogel and its use in a supercapacitor. Journal of Materials Chemistry A. 2013;**1**:208-211. DOI: 10.1039/C2TA00444E

[33] Samuels AJ, Carey JD. Engineering graphene conductivity for flexible and high-frequency applications. ACS Applied Materials & Interfaces. 2015;**7**:22246-22255. DOI: 10.1021/acsami.5b05140

[34] Jang MS, Brar VW, Sherrott MC, Lopez JJ, Kim L, Kim S, Choi M, Atwater HA. Tunable large resonant absorption in a midinfrared graphene Salisbury screen. Physical Review B. 2014;**90**:165409. DOI: 10.1103/PhysRevB.90.165409

[35] Cassabois G, Valvin P, Gil B. Hexagonal boron nitride is an indirect bandgap semiconductor. Nature Photonics. 2016;**10**:262-266. DOI: 10.1038/nphoton.2015.277

[36] Mak KF, Shan J. Photonics and optoelectronics of 2D semiconductor transition metal dichalcogenides. Nature Photonics. 2016;**10**:216-226. DOI: 10.1038/nphoton.2015.282

[37] XG Y, Marks TG, Facchetti A. Metal oxides for optoelectronic applications. Nature Materials. 2016;**15**:383-396. DOI: 10.1038/nmat4599

[38] Pizzi G, Gibertini M, Dib E, Marzari N, Iannaccone G, Fiori G. Performance of arsenene and antimonene double-gate MOSFETs from first principles. Nature Communications. 2016;**7**:12585. DOI: 10.1038/ncomms12585

[39] Khandelwal A, Mani K, Karigerasi MH, Lahiri I. Phosphorene–the two-dimensional black phosphorous: Properties, synthesis and applications. Materials Science and Engineering: B. 2017;**221**:17-34. DOI: 10.1016/j.mseb.2017.03.011

[40] Sichert JA, Tong Y, Mutz N, Vollmer M, Fischer S, Milowska KZ, Cortadella RG, Nickel B, Cardenas-Daw C, Stolarczyk JK, Urban AS, Feldmann J. Quantum size effect in organometal halide perovskite nanoplatelets. Nano Letter. 2015;**15**:6521-6527. DOI: 10.1021/acs.nanolett.5b02985

[41] Zhang YP, Liu JY, Wang ZY, Xue YZ, QD O, Polavarapu L, Zheng JL, Qia X, Bao QL. Synthesis, properties, and optical applications of low-dimensional perovskites. Chemical Communications. 2016;**52**:13637-13655. DOI: 10.1039/c6cc06425f

[42] Jeon T, Kim SJ, Yoon J, Byun J, Hong HR, Lee TW, Kim JS, Shin B, Kim SO. Hybrid perovskites: Effective crystal growth for optoelectronic applications. Advanced Energy Materials. 2017:1602596. DOI: 10.1002/aenm.201602596

[43] Sun SB, Yuan D, Xu Y, Wang AF, Deng ZT. Ligand-mediated synthesis of shape-controlled cesium lead halide perovskite nanocrystals via reprecipitation process at room temperature. ACS Nano. 2016;**10**:3648-3657. DOI: 10.1021/acsnano.5b08193

[44] Bekenstein Y, Koscher BA, Eaton SW, Yang PD, Alivisatos AP. Highly luminescent colloidal nanoplates of perovskite cesium lead halide and their oriented assemblies. Journal of American Chemical Society. 2015;**137**:16008-16011. DOI: 10.1021/jacs.5b11199

[45] Pan AZ, He B, Fan XY, Liu ZK, Urban JJ, Alivisatos AP, He L, Liu Y. Insight into the ligand-mediated synthesis of colloidal $CsPbBr_3$ perovskite nanocrystals: The role of organic acid, base, and cesium precursors. ACS Nano. 2016;**10**:7943-7954. DOI: 10.1021/acsnano.6b03863

[46] Shi YM, Li HN, Li LJ. Recent advances in controlled synthesis of two-dimensional transition metal dichalcogenides via vapour deposition techniques. Chemical Society Reviews. 2015;**44**:2744-2756. DOI: 10.1039/c4cs00256c

[47] Nayak PK, Horbatenko Y, Ahn S, Kim G, Lee JU, Ma KY, Jang AR, Lim H, Kim D, Ryu s CH, Park N, Shin HS. Probing evolution of twist-angle-dependent interlayer excitons in $MoSe_2/WSe_2$ van der Waals heterostructures. ACS Nano. 2017;**11**:4041-4050. DOI: 10.1021/acsnano.7b00640

[48] Ha ST, Liu XF, Zhang Q, Giovanni D, Sum TC, Xiong QH. Synthesis of organic–inorganic lead halide perovskite nanoplatelets: Towards high-performance perovskite solar cells and optoelectronic devices. Advanced Optical Materials. 2014;**2**:838-844. DOI: 10.1002/adom.201400106

[49] Xing GC, Mathews N, Sun SY, Lim SS, Lam YM, Grätzel M, Mhaisalkar S, Sum TC. Long-range balanced electron- and hole-transport lengths in organic-inorganic $CH_3NH_3PbI_3$. Science. 2013;**342**:344. DOI: 10.1126/science.1243167

[50] Wang YP, Shi YF, Xin GQ, Lian J, Shi J. Two-dimensional van der Waals expitaxy kinetics in a three-dimensional perovskite halide. Crystal Growth & Design. 2015;**15**:4741-4749. DOI: 10.1021/acs.cgd.5b00949

[51] Wang YL, Guan X, Li DH, Cheng HC, Duan XD, Lin ZY, Duan XF. Chemical vapor deposition growth of single-crystalline cesium lead halide microplatelets and heterostructures for optoelectronic applications. Nano Research. 2017;**10**:1223-1233. DOI: 10.1007/s12274-016-1317-1

[52] Wang Q, Li D, Cheng HC, Li Y, Chen CY, Yin A, Zhao Z, Lin Z, Wu H, He Q, Ding M, Liu Y, Huang Y, Duan X. Wafer-scale growth of large arrays of perovskite microplate crystals for functional electronics and optoelectronics. Science Advances. 2015;**1**:e1500613. DOI: 10.1126/sciadv.1500613

[53] Liu LG, Huang S, Pan LF, Shi LJ, Zou BS, Deng LG, Zhong HZ. Colloidal synthesis of $CH_3NH_3PbBr_3$ nanoplatelets with polarized emission through self-organization. Angewandte Chemie International Edition. 2017;**56**:1780-1783. DOI: 10.1002/anie.201610619

[54] Jodlowski AD, Yépez A, Luque R, Camacho L, de Miguel G. Benign-by-benign solventless mechanochemical synthesis of three-, two-, and one dimensional hybrid perovskites. Angewandte Chemie International Edition. 2016;**55**:14972-14977. DOI: 10.1002/anie.201607397

[55] Mitzi DB. Synthesis, crystal structure, and optical and thermal properties of $(C_4H_9NH_3)_2MI_4$ (M = Ge, Sn, Pb). Chemistry of Materials. 1996;**8**:791-800. DOI: 10.1021/cm9505097

[56] Calabrese J, Jones NL, Harlow RL, Herron N, Thorn DL, Wang Y. Preparation and characterization of layered lead halide compounds. Journal of American Chemical Society. 1991;**113**:2328-2330. DOI: 10.1021/ja00006a076

[57] Xu Z, Mitzi DB, Medeiros DR. $[(CH_3)_3NCH_2CH_2NH_3]SnI_4$: A layered perovskite with quaternary/primary ammonium dications and short interlayer iodine-iodine contacts. Inorganic Chemistry. 2003;**42**:1400-1402. DOI: 10.1021/ic0261981

[58] Tan ZJ, Wu Y, Hong H, Yin JB, Zhang JC, Lin L, Wang MZ, Sun X, Sun LZ, Huang YC, Liu KH, Liu ZF, Peng HL. Two-dimensional $(C_4H_9NH_3)_2PbBr_4$ perovskite crystals for high-performance photodetector. Journal of American Chemical Society. 2016;**138**:16612-16615. DOI: 10.1021/jacs.6b11683

[59] Stoumpos CC, Cao DH, Clark DJ, Young J, Rondinelli JM, Jang JI, Hupp JT, Kanatzidis MG. Ruddlesden-popper hybrid lead iodide perovskite 2D homologous semiconductors. Chemistry of Materials. 2016;**28**:2852-2867. DOI: 10.1021/acs.chemmater.6b00847

[60] Smith IC, Hoke ET, Solis-Ibarra D, McGehee MD, Karunadasa HI. A layered hybrid perovskite solar-cell absorber with enhanced moisture stability. Angewandte Chemie International Edition. 2014;**53**:11232-11235. DOI: 10.1002/anie.201406466

[61] Leng MY, Chen ZW, Yang Y, Li Z, Zeng K, Li KH, Niu GD, He YS, Zhou QC, Tang J. Lead-free, blue emitting bismuth halide perovskite quantum dots. Angewandte Chemie International Edition. 2016;**55**:15012-15016. DOI: 10.1002/anie.201608160

[62] Wang KH, Wu L, Li L, Yao HB, Qian HS, Yu SH. Large-scale synthesis of highly luminescent perovskite-related $CsPb_2Br_5$ nanoplatelets and their fast anion exchange. Angewandte Chemie International Edition. 2016;**55**:8328-8332. DOI: 10.1002/anie.201602787

[63] Vargas B, Ramos E, Pérez-Gutiérrez E, Alonso JC, Solis-Ibarra D. A direct bandgap copper-antimony halide perovskite. Journal of American Chemical Society. DOI: 10.1021/jacs.7b04119

[64] Levchuk I, Herre P, Brandl M, Osvet A, Hock R, Peukert W, Schweizer P, Spiecker E, Batentschuk M, Brabec CJ. Ligand-assisted thickness tailoring of highly luminescent colloidal $CH_3NH_3PbX_3$ (X = Br and I) perovskite nanoplatelets. Chemical Communications. 2017;**53**:244-247. DOI: 10.1039/c6cc09266g

[65] Zhang Q, Su R, Liu XF, Xing J, Sum TC, Xiong QH. High quality whispering-gallery-mode lasing from cesium lead halide perovskite nanoplatelets. Advanced Functional Materials. 2016;**26**:6238-6245. DOI: 10.1002/adfm.201601690

[66] Zhang Q, Ha ST, Liu XF, Sum TC, Xiong QH. Room-temperature near-infrared high-Q perovskite whispering-gallery planar nanolasers. Nano Letter. 2014;**14**:5995-6001. DOI: 10.1021/nl503057g

[67] Liao Q, Hu K, Zhang HH, Wang XD, Yao JN, Fu HB. Perovskite microdisk microlasers self-assembled from solution. Advanced Materials. 2015;**27**:3405-3410. DOI: 10.1002/adma.201500449

[68] Dou L, Wong AB, Yu Y, Lai M, Kornienko N, Eaton SW, Fu A, Bischak CG, Ma J, Ding T, Ginsberg NS, Wang LW, Alivisatos AP, Yang P. Atomically thin two-dimensional organic-inorganic hybrid perovskites. Science. 2015;**349**:1518-1521. DOI: 10.1126/science.aac7660

[69] Yang S, Niu WX, Wang AL, Fan ZX, Chen B, Tan CL, Lu QP, Zhang H. Ultrathin two-dimensional organic–inorganic hybrid perovskite nanosheets with bright, tunable photoluminescence and high stability. Angewandte Chemie International Edition. 2017;**56**:1-5. DOI: 10.1002/adma.201605448

[70] Akkerman QA, Motti SC, Kandada ARS, Mosconi E, D'Innocenzo V, Bertoni G, Marras S, Kamino BA, Miranda L, Angelis FD, Petrozza A, Prato M, Manna L. Solution synthesis approach to colloidal cesium lead halide perovskite nanoplatelets with monolayer-level thickness control. Journal of American Chemical Society. 2016;**138**:1010-1016. DOI: 10.1021/jacs.5b12124

[71] Billing DG, Lemmerer A. Synthesis, characterization and phase transitions in the inorganic-organic layered perovskite-type hybrids [$(C_nH_{2n+1}NH_3)_2PbI_4$], n = 4, 5 and 6. Acta Crystallographic Section B: Structural Science. 2007;**63**:735-747. DOI: 10.1107/S0108768107031758

[72] Dohner ER, Jaffe A, Bradshaw LR, Karunadasa HI. Intrinsic white-light emission from layered hybrid perovskites. Journal of American Chemical Society. 2014;**136**:13154-13157. DOI: 10.1021/ja507086b

[73] Cortecchia D, Neutzner S, Kandada ARS, Mosconi E, Meggiolaro D, Angelis FD, Soci C, Petrozza A. Broadband emission in two-dimensional hybrid perovskites: The role of structural deformation. Journal of American Chemical Society. 2017;**139**:39-42. DOI: 10.1021/jacs.6b10390

[74] Zhou JC, Chu YL, Huang J. Photodetectors based on two-dimensional layer-structured hybrid lead iodide perovskite semiconductors. ACS Applied Materials & Interfaces. 2016;**8**:25660-25666. DOI: 10.1021/acsami.6b09489

[75] Li MQ, YQ H, Bi LY, Zhang HL, Wang YY, Zheng YZ. Structure tunable organic-inorganic bismuth halides for an enhanced two-dimensional lead-free light-harvesting material. Chemistry of Materials. DOI: 10.1021/acs.chemmater.7b01017

[76] Song JZ, LM X, Li JH, Xue J, Dong YH, Li XM, Zeng HB. Monolayer and few-layer all-inorganic perovskites as a new family of two-dimensional semiconductors for printable optoelectronic devices. Advanced Materials. 2016;**28**:4861-4869. DOI: 10.1002/adma.201600225

[77] Liu JY, Xue YZ, Wang ZY, Xu ZQ, Zheng CX, Weber B, Song JC, Wang YS, Lu YY, Zhang YP, Bao QL. Two-dimensional $CH_3NH_3PbI_3$ perovskite: Synthesis and optoelectronic application. ACS Nano. 2016;**10**:3536-3542. DOI: 10.1021/acsnano.5b07791

[78] Lv LF, YB X, Fang HH, Luo WJ, FJ X, Liu LM, Wang BW, Zhang XF, Yang D, WD H, Dong AG. Generalized colloidal synthesis of high-quality, two-dimensional cesium lead halide perovskite nanosheets and their applications in photodetectors. Nanoscale. 2016;**8**:13589-13596. DOI: 10.1039/c6nr03428d

[79] Li PF, Shivananju BN, Zhang YP, Li SJ, Bao QL. High performance photodetector based on 2D $CH_3NH_3PbI_3$ perovskite nanosheets. Journal of Physics D: Applied Physics. 2017;**50**:094002. DOI: 10.1088/1361-6463/aa5623

[80] Stan A, Dahlen NE, Leeuwen RV. Levels of self-consistency in the GW approximation. The Journal of Chemical Physics. 2009;**130**:114105. DOI: 10.1063/1.3089567

[81] Imamura Y, Nakai H. Time-dependent density functional theory (TDDFT) calculations for core-excited states: Assessment of an exchange functional combining the Becke88 and van Leeuwen–Baerends-type functionals. Chemical Physics Letters. 2006;**419**:297-303. DOI: 10.1016/j.cplett.2005.11.084

[82] Wen XD, Martin RL, Scuseria GE, Rudin SP, Batista ER, Burrell AK. Screened hybrid and DFT + U studies of the structural, electronic, and optical properties of U_3O_8. Journal of Physics: Condensed Matter. 2013;**25**:025501. DOI: 10.1088/0953-8984/25/2/025501

[83] Betzinger M, Friedrich C, Blügel S. Hybrid functionals within the all-electron FLAPW method: implementation and applications of PBE0. Physical Review B. 2010;**81**:195117. DOI: 10.1103/PhysRevB.81.195117

[84] Gavnholt J, Olsen T, Engelund M, Schiøtz J. Delta self-consistent field as a method to obtain potential energy surfaces of excited molecules on surfaces. Physical Review B. 2008;**78**. DOI: 075441, 10.1103/PhysRevB.78.075441

[85] Yang DW, Lv J, Zhao XG, QL X, YH F, Zhan YQ, Zunger A, Zhang LJ. Functionality-directed screening of Pb-free hybrid organic-inorganic perovskites with desired intrinsic photovoltaic functionalities. Chemistry of Materials. 2017;**29**:524-538. DOI: 10.1021/acs.chemmater.6b03221

[86] Chen JS, Žídek K, Chábera P, Liu DZ, Cheng PF, Nuuttila L, Al-Marri MJ, Lehtivuori H, Messing ME, Han KL, Zheng KB, Pullerits T. Size- and wavelength-dependent two-photon absorption cross-section of $CsPbBr_3$ perovskite quantum dots. The Journal of Physical Chemistry Letters. 2017;**8**:2316-2321. DOI: 10.1021/acs.chemmater.6b03221